Key Points:
- The dependence of the structure of magnetotail dipolarization jets on cross-tail width is studied through 2-D Riemann simulations
- For small widths the jet velocity falls well below expectations based on predictions of conventional reconnection models
- In wide jets the self-generated Hall magnetic field reverses sign compared with traditional predictions on the dawn edge of the jet

Correspondence to:
H. Arnold,
harryarnold@gmail.com

Characterizing Ion Flows Across a Magnetotail Dipolarization Jet

H. Arnold[1] [ID]**, M. Swisdak[1]** [ID]**, and J. F. Drake[1]** [ID]

[1] IREAP, University of Maryland, College Park, MD, USA

Abstract The structure of dipolarization jets with finite width in the dawn-dusk direction relevant to magnetic reconnection in the Earth's magnetotail is explored with particle-in-cell simulations. We carry out Riemann simulations of the evolution of the jet in the dawn-dusk, north-south plane to investigate the dependence of the jet structure on the jet width in the dawn-dusk direction. We find that the magnetic field and Earth-directed ion flow structure depend on the dawn-dusk width. A reversal in the usual Hall magnetic field near the center of the current sheet on the duskside of larger jets is observed. For small widths, the maximum velocity of the earthward flow is significantly reduced below the theoretical limit of the upstream Alfvén speed. However, the ion flow speed approaches this limit once the width exceeds the ion Larmor radius based on the normal magnetic field, B_z.

Plain Language Summary Magnetic reconnection is a phenomenon occurring in the Earth's magnetotail in which energy stored in the magnetic field is converted into kinetic energy. This process creates a high-speed *dipolarization jet* of plasma. However, the physical dimension of these jets in the dawn-dusk direction is not well constrained. We study how the structure of dipolarization jets depends on their width in the dawn-dusk direction and find that both the shape of the magnetic field and the profile of the ion outflow speed across the jet vary as a function of the jet width. In particular, the maximum ion outflow can fall well short of the theoretically expected outflow speed for small widths. Our results can be used by satellites to determine their positions relative to observed dipolarization jets and place limits on the jet widths.

1. Introduction

Magnetic reconnection is a common phenomenon in the Earth's magnetotail, solar flares, coronal mass ejections, and sawtooth crashes in tokamaks; as such, it is a subject of active research. When two oppositely directed field lines reconnect, energy stored in the magnetic field is transferred to particle energy (Angelopoulos et al., 2008). The particles are accelerated by the tension in the reconnected field lines in two oppositely directed jets away from the x-line, the location where the reconnecting component of the field vanishes. In the case of the magnetotail, reconnection causes one jet to move earthward and the other to be directed tailward. While it has been shown that the Alfvén speed is the maximum speed to which these dipolarization jets can accelerate flows (Parker, 1957), it is unclear how the extent of the jet in the dawn-dusk direction affects this result.

Reconnection begins at the x-line, and many studies have examined the ion and electron dissipation regions centered around it. We focus farther downstream on the structure of the dipolarization jet. Previous 2-D simulations (e.g., Sitnov & Swisdak, 2011; Wu & Shay, 2012) have frequently focused on the *x-z* plane [in Geocentric Solar Magnetospheric coordinates (GSM)] and have examined the snowplow-like behavior of the dipolarization front as it sweeps up plasma during its earthward motion. Such simulations implicitly assume that the dipolarization jet has infinite extent in the *y* direction. Performing fully 3-D simulations lifts this restriction. Several authors have recently performed such simulations (Drake et al., 2014; Pritchett, 2015; Pritchett et al., 2014; Sitnov et al., 2014, 2017). Generally speaking, they find that the full dimensionality allows for more complicated dynamics and the self-consistent development of fine-scale structure in the dawn-dusk direction that results from the development of strong flows associated with interchange dynamics. These interchange-driven flows are sensitive to the initial tail equilibrium and specifically the profile of

the north-south magnetic field B_z in the downtail direction. That such interchange-driven flows dominate the magnetotail dynamics has not been established with detailed comparisons with observations.

To avoid the uncertainties associated with the cross-tail jet structure, Drake et al. (2014) studied a three-dimensional Riemann-like system in which the cross-tail width of the jet was specified as an initial condition. They found that the bulk kinetic energy of the jet was dissipated at the jet front as a result of the reflection of ions off the front, bending the front in the dusk direction. Alternatively, a current blocking mechanism was implemented by Pritchett (2015) to explore the development of large-scale, reconnection-driven jets of various cross-tail widths. These 3-D simulations also revealed reconnection jets that are extended in the *x* direction but with very strong deflection of the fronts of the jets in the duskward direction. Thus, the results of 3-D particle-in-cell (PIC) simulations have not yet converged on a uniform picture of how large-scale, reconnection-driven jets in the magnetotail develop.

In the 3-D simulations of Drake et al. (2014) the core of the jet, well away from the front (in the *x* direction), was fairly laminar with minimal variation in the *x* direction. This suggests that simulations in a two-dimensional plane (north-south and dawn-dusk) could serve as a useful model for exploring the structure of the body of the jet (for a full explanation of why such a 2-D simulation is a reasonable approach; see the supporting information). In the present manuscript we use such simulations to explore dependence of the structure of the core of magnetotail magnetic reconnection jets (away from the jet front) on their finite extent in the cross-tail direction and, in particular, how this determines the profile of the earthward directed ion flow and the structure of the Hall magnetic fields in the cross-tail direction. To be clear, we are not addressing the physics of reconnection onset in the magnetotail and the mechanisms that control the finite extent (in *y*) of these jets nor are we attempting to model the entire magnetotail. Thus, we initialize B_z (and all other quantities) as constants with respect to *x* and not decreasing with distance from Earth, as would be appropriate in a global simulation of the full magnetotail. The jet width in the cross-tail direction is specified as an initial condition (Drake et al., 2014). The current blocking method (Pritchett, 2015) is an alternative approach for controlling the cross-tail width of the jet and the dipolarization front. In our approach we are not concerned with how reconnection proceeds but focus instead on the cross-tail structure of the jet core. The goal is to establish signatures associated with the finite cross-tail jet structure that could be compared with the observations. Finally, we emphasize that the structure of the jet core is important because this is where most of the magnetic energy released during reconnection drives the ion bulk flow and ion thermal heating, which dominate the energetics of reconnection in the magnetotail (Eastwood et al., 2013).

During reconnection in the magnetotail, ions are accelerated toward the Earth and down the tail by the newly reconnected magnetic fields. To accelerate up to the Alfvén speed, they first move in the cross-tail direction, the direction of the reconnection electric field, before they turn toward or away from the Earth. It is not a surprise, therefore, that in very narrow jets the ions are unable to gain enough energy to reach the Alfvén speed. In this manuscript we quantify the relation between the peak ion earthward flow and the cross-tail width of the jet.

That the finite cross-tail width of the jet can impact the Hall magnetic field is more surprising. It is well known from theory, simulations, and observations that Hall magnetic fields are produced near the x-line (Mandt et al., 1994; Øieroset et al., 2001; Sonnerup, 1979). These fields arise because they are primarily frozen-in to the electrons inside of the ion diffusion region. Thus, the electrons, which are carrying the current in the current sheet, enter the ion diffusion region and push on the fields, bending the reconnection magnetic field into the out-of-plane direction. Simulations indicate that these Hall fields are carried far downstream, $\sim$100 d_i, from the x-line (Le et al., 2010, 2014; Shay et al., 2011), especially away from the center of the current sheet. We find that the Hall fields reverse inside of the current sheet for large widths in the dawn-dusk direction. However, these fields do return to the expected orientation away from the current sheet. This effect is due to the ions from the current sheet pushing on the field lines in the opposite direction of the electrons.

2. Simulations

We use the PIC code `p3d` (Zeiler et al., 2002). The magnetic field strength B_0 and density n_0 define the Alfvén speed $V_A = \sqrt{B_0^2/4\pi m_i n_0}$, with lengths normalized to the ion inertial length $d_i = c/\omega_{pi}$, where ω_{pi} is the ion plasma frequency and times to the ion cyclotron time Ω_{i0}^{-1}. Electric fields and temperatures are normalized to $V_A B_0/c$ and $m_i V_A^2$, respectively. The coordinate system for all simulations is geocentric solar magnetospheric.

The initial conditions for the simulations are intended to mimic those of a dipolarization jet and are similar to Riemann simulations such as Scholer and Lottermoser (1998) in that we have no x-line in our domain. We start with a classical Harris current sheet with an asymptotic magnetic field B_0, central density n_0, and uniform background density $n_b = 0.3n_0$. To this equilibrium, we add a region of $B_z = 0.2B_0 \exp[-(y/w)^8]$, where w is the width. We choose to raise the exponent to the eighth power to localize the jet in the dawn-dusk (y) direction. The corresponding plasma density has a y dependence of $n = n_b + n_0(1 - \exp[-(y/w)^8])$. Thus, the density in the jet is roughly the lobe density, n_b, and outside it is the typical Harris current sheet density, $n = n_b + n_0$. The intent is to depict late-time tail reconnection in which the jet is formed from heated lobe plasma. Hence, in the region with B_z nonzero, the field is nonzero at the symmetry (equatorial) plane. In order to maintain pressure balance, we modify the electron and ion temperatures in the jet. The asymptotic temperatures, in code units, are 1/12 and 5/12 for the electrons and ions, respectively. The ion-to-electron mass ratio is set to 25, which is sufficient to separate the electron and ion scales. The current is determined from Ampère's law with no displacement current and is divided between ions and electrons in proportion to their temperatures in all regions. All the forces are balanced in the y and z directions, but there is an unbalanced force in the x direction due to a non zero $B_z \partial_z B_x$ term in the fluid momentum equation. This force accelerates the plasma toward the Earth in the magnetotail. Following initialization, the system adjusts and reaches a quasi-steady configuration as in a conventional Riemann model.

We perform quasi-two-dimensional (quasi-2-D) simulations with two full spatial dimensions (y and z). The addition of a small spatial extent in x reduces particle noise once the simulation data are averaged over all cells in the x direction. Note that no organized structure develops along x and that periodicity in this direction guarantees that the boundary conditions along x do not introduce any spurious numerical artifacts. These simulations allow us to explore the late-time, cross-tail structure of jets of various widths. Typical simulation dimensions are $(x, y, z) = (3.2, 102.4, 102.4)d_i$. We also compare the results of our 2-D simulation with a full 3-D simulation with $(x, y, z) = (102.4, 25.6, 25.6)d_i$, which has already been discussed in Drake et al. (2014). The spatial grid has a resolution $\Delta = 0.05$, while the smallest physical scale is the Debye length in the magnetotail, ≈ 0.03. We use 100 particles per cell per species for the simulations with a small extent in x. The simulation with a larger extent in x uses 50 particles per cell. In all simulations the speed of light is $c = 15$ and we employ periodic boundary conditions in all directions, which is a standard approach in simulations of magnetic reconnection. (Note that periodicity in z actually requires us to simulate two mirror-image current sheets. We stop the simulation before the two current sheets begin to interact and only present results from one. Both sheets undergo very similar evolution.) The widths, w, we examine are as follows: $\sim 1d_i$, $\sim 2d_i$, $\sim 3d_i$, $\sim 4d_i$, $\sim 7d_i$, $\sim 15d_i$, $\sim 30d_i$, and infinite (occupying the full space along y). For a full comparison between the quasi-2-D simulations and the full 3-D version see the supporting information.

3. Presentation and Analysis of Simulation Results

3.1. Reversal of the Hall Field

As a result of the system's evolution, the Hall magnetic field (B_y) on the dusk edge of the jet reverses sign from its usual direction, especially for jets with a large width. Figure 1 is an image of the total current in the x direction for the simulation with the largest finite width dipolarization jet, $w \sim 30d_i$. Overlaid are arrows showing the in-plane ion flows and magnetic field lines in shades of green. For clarity, additional figures can be found in Text S1 in the supporting information. The current layer can be identified by the ions flowing duskward ($-2 \leq z/d_i \leq 2$). The electrons (not shown) primarily flow dawnward within the current sheet. The ends of the field lines are evenly distributed along the bottom of the jet in z and are followed until they leave the area depicted in Figure 1. Below the 2-D image is a cut through the center of the current sheet of the ion current in the y direction.

On the dawn (left) side of the jet the electrons carry the magnetic field to the left and produce the usual sign of the Hall magnetic field B_y (negative below the center of the current sheet and positive above). The small dimple on the extreme dawn edge is likely due to ions carrying the field toward the dusk.

On the dusk (right) side of the jet, however, B_y reverses sign compared with the usual Hall magnetic field, as is visible above and below the center of the current sheet in Figure 1. Early in this simulation (not shown) the field is initially dragged dawnward by the electrons before reversing, indicating that even with some initial Hall field of the standard sign, the ions will still reverse the direction by late times. The reversal, in this case, arises due to ions pushing on the field as a result of the vortex pair that forms just duskward of the jet and is
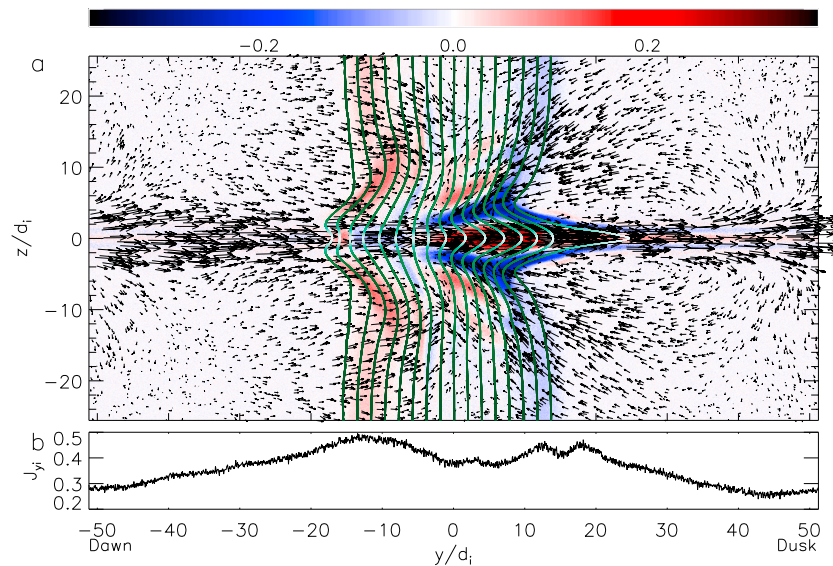
Figure 1. (a) The x component of the total current in the y-z plane at $\Omega_{i0}t = 40$ for a dipolarization jet of width $\approx 30d_i$. Plotted in black arrows are ion flow vectors with the length proportional to the magnitude of the velocity. The in-plane magnetic field lines in the jet are displayed in green, with darker shades indicating a stronger magnetic field. (b) A cut of the total ion current in the y direction through the center of the current sheet ($z/d_i = 0$).

observed to begin around $\Omega_{i0}t \approx 20$. The vortex pair consists of two adjacent vortices that are centered just above and below the current layer. Their vorticities have opposite signs so their flows add at the center of the current layer. The resulting strong duskward ion flow near the center of the current sheet carries the field lines toward the dusk, while the return (dawnward) ion flow above and below the current sheet carries the field lines toward the dawn. The result is a reversal in the Hall field just above and below the center of the current sheet with the sign of B_y taking the usual values further away from the current sheet.

We now discuss the mechanism for the development of the vortex pair. In the initial state the ions flow uniformly across the domain toward the dusk. The imposed B_z diverts the flowing ions toward the Earth, which slows their duskward flow. The flowing ions outside of the jet on the duskside continue to flow toward the dusk and try to fill in this depletion by turning back toward the jet, thereby forming the two vortices evident in Figure 1a. The reduction of the ion current shown in the cut along the middle of the current layer in Figure 1b over the interval $20 < y/d_i < 40$ results from the diversion of the ion flow away from the current layer as seen in the velocity vectors of Figure 1a.

The ions in the jet contribute to closing these ion vortices. As time progresses, the tension in the *reconnected* magnetic field (in the z-x plane) drives the plasma flow in the positive x (earthward) direction. This motion causes ions in the lobes to move toward the current sheet and produces the converging flows (toward $z = 0$) seen on the duskward edge of the jet. Upon entering the current sheet, the ions move in Speiser-like orbits and rotate first into the positive y direction before completing their Speiser motion into earthward flow. Their motion in the duskward direction as they rotate in the current layer contributes to the enhancement in J_{iy} seen around $y/d_i \sim 15$ in Figure 1b. This high-speed ion flow carries the magnetic field duskward and drives the reversed Hall field seen in the data.

An organized reversal in the Hall magnetic field has not been seen even in large-scale 2-D reconnection simulations (carried out in the x-z plane; Le et al., 2010, 2014; Shay et al., 2011) although firehose-driven turbulence in the jet can produce local reversals of B_y (Hietala et al., 2015). An important question then is whether these earlier results are consistent with the Hall field reversal seen in the present simulations with the largest jet width. Since nearly all of the ions in dipolarization jets originate upstream in the lobes, they carry little cross-tail momentum as they enter the jet and total momentum conservation in the cross-tail direction means that they will not gain a significant net flow in the cross-tail direction (Liu et al., 2012). It is therefore the electrons that carry most of the cross-tail current in 2-D reconnection simulations. An infinite width jet would, of course, not produce the vortex shown in Figure 1a since $\partial_y = 0$. Thus, we would not expect the Hall field to reverse for jets with infinite extent in the cross-tail direction. To confirm this, we performed a separate simulation with an
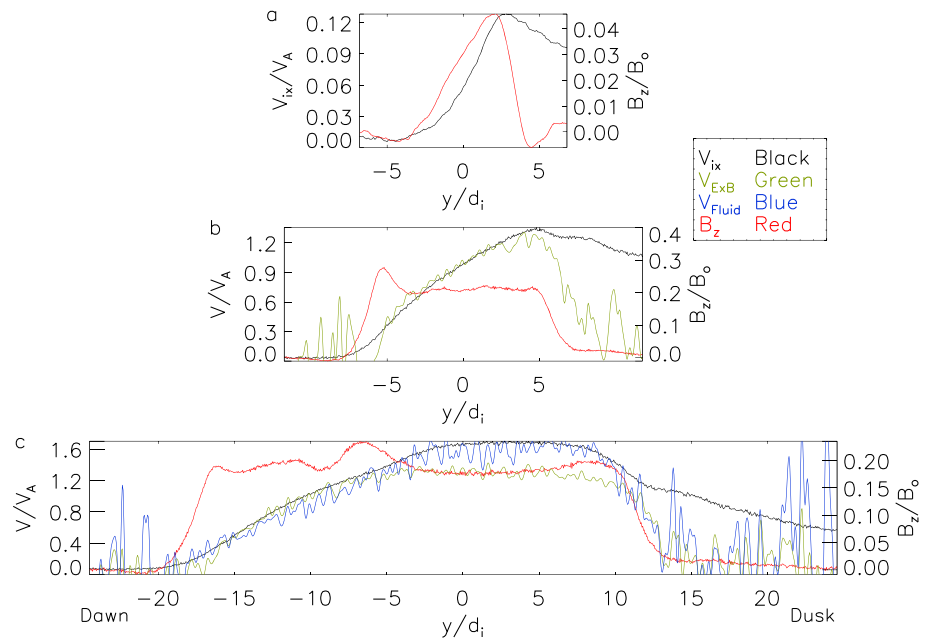
Figure 2. The x component of the ion velocity (black) and the z component of the magnetic field (red) from three runs at $\Omega_{i0}t = 40$ along a cut taken at $z = 0$. Panels (b) and (c) also include the local $\mathbf{E} \times \mathbf{B}$ velocity in the x direction (green). Finally v_{fluid} (blue), described in the text, is plotted for panel (c). (a) The smallest jet, width $\sim 1d_i$, (b) a medium-sized jet, width $\sim 15d_i$, and (c) the largest finite jet, width $\sim 30d_i$. The images only show a portion of the full simulated space. Note that the smallest jet has significantly increased in width at late times, but that there is a corresponding decrease in the magnetic field to compensate. For this reason the $\mathbf{E} \times \mathbf{B}$ velocity is too noisy to be seen, and thus, we have omitted it from this figure.

infinite jet with only the electrons carrying the initial current. At late times there was a nonzero duskward flow of ions, but it was significantly smaller than the ion flow depicted in Figure 1 and was unable to reverse the Hall field. This result is consistent with past 2-D reconnection simulations that did not see a reversal of the Hall field. Additionally, a reduction in the ion outflow speed of $\approx 60\%$ was observed. This is due to regions of the jet being firehose unstable as explained in Liu et al. (2012) and Haggerty et al. (2018). Our simulations with a finite width also include this effect; however, the reversal of the Hall field plays an important role in boosting the outflow speed as explained in the next section.

3.2. The Dependence of the Earthward Directed Flow on Cross-Tail Width

Figure 2 shows the earthward directed ion flow velocity in black through the center of the current sheet ($z/d_i = 0$) for jets with widths of $\sim 1d_i$, $\sim 15d_i$, and $\sim 30d_i$. For clarity, the magnetic field profile is also shown in red. For Figures 2b and 2c the local $\mathbf{E} \times \mathbf{B}$ drift velocity is also plotted in green (we neglect this for Figure 2a since it is too noisy) as well as a quantity v_{Fluid} described below for Figure 2c. Though not shown, the reconnection electric field $E_y = V_{E \times B}B_z$ follows the profile of $V_{E \times B}$ because B_z is nearly constant within the jet. Figure 2c clearly shows the four phases of the ion outflow along the cross-tail direction, y. First, the ions enter the dawnward side of the jet with no flow in the x direction. Second, upon entering the jet, the ions accelerate along the reconnection electric field E_y, which increases with distance into the jet, and rotate into the x or $\mathbf{E} \times \mathbf{B}$ drift direction. Third, these ions continue to drift duskward due to the curvature of the magnetic field and mix with ions from the lobes to form an earthward flow at the upstream Alfvén speed. In the fourth phase the ions have drifted out of the jet and retain their x directed motion since they are moving along the unreconnected magnetic field B_x. Outside of the jet, the ions mix with the background population so that the outflow speed slowly decays with increasing distance from the jet. Note that, although only the simulation shown in Figure 2c with $w = 30d_i$ is sufficiently large enough to exhibit the plateau, all three simulations produce an earthward directed, magnetic-field-aligned beam of ions in a region with $B_z = 0$.

To understand the scale length of the region where the ions are accelerating, consider that the ion outflow speed plateaus at the upstream Alfvén speed. Thus, we can make the following scaling argument starting

with the steady state ion conservation of momentum equation for a 2-D system ($\partial_x = 0$) at $z = 0$:

$$mnv_{yi}\partial_y v_{xi} \approx \frac{B_z}{4\pi}\partial_z B_x \sim mnv_{yi}\frac{C_A}{L_y} \sim \frac{B_z}{4\pi}\frac{B_x}{\Delta} \tag{1}$$

where C_A is the upstream Alfvén speed, L_y is the acceleration length scale, Δ is the half width of the current sheet, and $v_{zi} = 0$ due to the symmetry of the configuration. We neglect the divergence of the pressure since it is smaller than the magnetic tension in the region of interest. Next, since the ions carry most of the current on their entry into the jet, we can approximate v_y from Ampère's law on the dawnside of the jet:

$$\partial_z B_x = \frac{4\pi}{c}nqv_{yi} \sim B_x/\Delta \tag{2}$$

Then, plugging v_y into equation (1), solving for L_y, and normalizing to code units, we obtain:

$$L_y/d_i \sim \sqrt{\frac{n_0}{n_b}}\frac{B_x}{B_z}, \tag{3}$$

where n_b is the upstream ion density. For our simulation, $n_b/n_0 \approx 0.3$ and $B_x/B_z \approx 5$ giving $L_y/d_i \sim 10$, which is in agreement with Figure 2c and explains why Figure 2b, which only has a width of approximately $10d_i$, has no plateau.

While the $\mathbf{E} \times \mathbf{B}$ drift describes the motion of the ions for medium sized and smaller jets (e.g., Figure 2b), it falls short of accurately depicting the ion motion for larger jets after they plateau in speed. Thus, it is of interest to evaluate whether the particle motion within a dipolarization jet can be described by the usual guiding center drifts. A quantitative test comes from evaluating the κ parameter of Büchner and Zelenyi (1989). Defined as $\kappa = \sqrt{R_{min}/\rho_{max}}$, where R_{min} is the minimum radius of curvature and ρ_{max} is a particle's maximum Larmor radius. Values greater than unity are associated with well-behaved trajectories (i.e., well described by drifts). For our simulations we find κ for the ions to be $\lesssim 1$ within the jets. Thus, we cannot expect the guiding center drifts to accurately describe the observed flows seen in Figure 2. Nevertheless, the underlying physics driving the drifts (curvature of the magnetic field, magnetic field gradients, etc.) will still influence the particle flows.

Although there is some agreement between the $\mathbf{E} \times \mathbf{B}$ drift and the ion flow, there must be additional physics at work in the region where they diverge (e.g., for $-5 \leq y/d_i \leq 10$ in Figure 2c). By manipulating the ion momentum equation perpendicular to the magnetic field and neglecting the ion inertia terms, we can write:

$$v_{\text{Fluid}} = \frac{c}{B^2}\mathbf{E} \times \mathbf{B} + \frac{c}{qnB^2}\mathbf{B} \times \nabla \cdot \bar{\bar{P}}, \tag{4}$$

where v_{Fluid} is the velocity of the ion fluid perpendicular to the magnetic field and is the sum of the $\mathbf{E} \times \mathbf{B}$ drift and the pressure tensor effects. We have plotted this quantity in Figure 2c, and it matches the observed flow as expected. Note that we did not plot this quantity for Figures 2a and 2b since it closely matches the $\mathbf{E} \times \mathbf{B}$ drift. To understand if this is a result of a diamagnetic like drift, v_*, we calculated the trace of the pressure tensor, P_{trace}, and found that the following quantity is negligible:

$$v_* = -\frac{c}{qnB^2}\nabla P_{\text{trace}} \times \mathbf{B} \tag{5}$$

a likely source for the nonzero divergence of the pressure tensor. Recall from Figure 1 that the Hall field reverses around $y/d_i \sim -3$ creating field lines bent duskward. This is also where the ion flow diverges from the $\mathbf{E} \times \mathbf{B}$ drift indicating that the curvature of the magnetic field boosts the ion flow in the x direction. Direct calculation of the curvature drift leads to ion flow velocities significantly larger than observed (although of the correct sign). However, because $\kappa \lesssim 1$, the particle orbits are not well described by drifts superimposed on circular Larmor orbits and agreement should not be expected.

It should be noted that although the jet in Figure 2b has a width ~ 2 times greater than that of Figure 2a at the time shown, the jet widths at $t = 0$ differ by a factor of ~ 15. The widening of the jet in Figure 2a is accompanied by a drop in B_z, so that the integrated magnetic flux is constant. Once the simulation begins, the electrons, as the less massive species, interact with the fields first. The electrons in the region inside of the jet initially have a large velocity in the dawn direction and a low density compared to the electrons in the current sheet outside of the jet. Hence, the electrons in the jet carry the magnetic flux B_z in the jet toward the dawn, while the electrons entering the jet from the dusk carry the flux with a lower velocity. The resulting divergence of
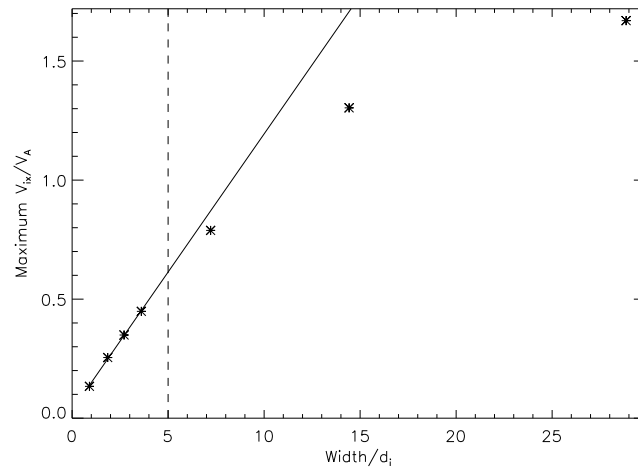
Figure 3. The x component of the maximum ion flow velocity inside the jet versus the width. The linear fit shown in this figure (solid) was calculated from the first four data points. Widths greater than the local Larmor radius (dashed), $\sim 5d_i$, are no longer linear.

the cross-tail electron flow spreads the flux as seen in Figure 2a and leads to a buildup of magnetic flux on the dawn (left) side for larger jets. This effect leads to the smallest initial-width jet achieving a width comparable to the medium sized jet (Figures 2a and 2b).

3.3. Maximum Ion Flow Dependence on Jet Width

It is well known that the ion flow in a dipolarization jet can be accelerated to the upstream Alfvén speed in a jet that has infinite cross-tail width. For the case of a finite width jet we have shown that there is a transition between the nearly zero ion flow outside of the jet on the dawnside and where the flow reaches the maximum outflow speed. An ion in the current sheet enters a region of nonzero B_z and E_y from the dawnside and gains an $\mathbf{E} \times \mathbf{B}$ drift in the x direction. It is reasonable to expect that jets with a width less than the ion Larmor radius in the magnetic field, B_z, would be unable to fully accelerate the ions to this maximum speed since they would leave the jet before completing a full orbit. In our simulations the ions have a local Larmor radius of $\sim 5d_i$ (due to B_z) in the center of the jet. We start from equation (1). Since the jet widths are short, the ion velocity v_{yi} inside the jet is nearly unchanged from that outside so v_{yi} is again given in equation (2). The resulting equation for v_{xi} is as follows:

$$mn \left(\frac{c \partial_z B_x}{4\pi nq} \right) \frac{\partial v_{xi}}{\partial y} \approx \frac{B_z}{4\pi} \partial_z B_x \sim mn \left(\frac{cB_x}{4\pi nq\Delta} \right) \frac{\partial v_{xi}}{\partial y} \sim \frac{B_z B_x}{4\pi\Delta}, \tag{6}$$

where Δ is the half width of the current sheet. The equation can be integrated to obtain the increase in v_{xi} with distance inside of the jet. However, the integral is complicated by the fact that B_z spreads in time as shown in Figure 2. Fortunately, the total magnetic flux associated with B_z is a constant and is given by $B_{z0}w$, where B_{z0} is the initial value of B_z. Completing the integral, we obtain the maximum ion flow speed inside the dipolarization jet $v_{xi,\max}$. In normalized code units the result is given by

$$\frac{v_{xi,\max}}{V_A} \sim \frac{B_{z0}}{B_x} \frac{w}{d_i}. \tag{7}$$

Taking values from the simulations for $B_z(= 0.2)$, and $B_x(= 1)$, we arrive at a slope of 0.2 for $v_{xi,\max}/V_A$ versus w/d_i. Figure 3 shows the relationship between the maximum outflow velocity and the width w. A linear fit to the first few data points gives a slope of ~ 0.12, which differs by less than a factor of 2 from our simple model. At larger widths, the jet velocity approaches the upstream Alfvén speed with increasing w. The simulation results begin to deviate from the linear relationship for the simulation with $w = 7d_i$, suggesting that other physical effects become important around this length scale. This is expected since the data from $w = 4d_i$ and $w = 7d_i$ bracket the local ion Larmor radius of $5d_i$ in the jet (i.e., bracket the length scale at which we expect our model to break down). For w well above $\sim 5d_i$ the maximum v_{ix} then approaches the upstream Alfvén speed, $\sim 1.8 V_A$. Figure 3 clearly shows the strong dependence of the speed of the flow on the width of the jet.

4. Conclusion

We use quasi-2-D PIC simulations to analyze the structure of the ion outflow and magnetic field on the dawn-dusk width of a dipolarization jet. For large, finite widths there is a significant reversal in the Hall magnetic field on the duskside of the jet. This reversal, which should be detectable by spacecraft observations, results from the interaction of duskward moving ions with the magnetic field and results in the generation of a y component of the magnetic field. The reversal happens approximately, where the x component of the ion flow reaches a maximum inside the jet and is supported by vortices above and below the current sheet that extend outside of the jet on the duskside. The reversal of the Hall magnetic field does not appear for jets that have infinite extent in the cross-tail direction, which is consistent with simulations of symmetric reconnection that reveal Hall magnetic fields of the normal sign far downstream from the x-line (Le et al., 2010, 2014; Shay et al., 2011) and simulations that do not show any coherent behavior near the current sheet (Hietala et al., 2015). The bent field lines shown in our simulations are due to the ions moving with high velocity in the dusk direction bending the magnetic field B_z into the cross-tail direction. This behavior does not appear in 2-D models of reconnection because the ions initially in the current sheet, and which carry large momentum in the cross-tail direction, are swept downstream in a plasmoid (Arzner & Scholer, 2001) leaving only a population of ions from the lobes inside the jet. These ions are unable to interact with the current sheet and form a flow with a high enough cross-tail speed to reverse the Hall field.

In addition, we were able to demonstrate that there is a strong dependence of the maximum earthward flow on the width of a dipolarization jet in the dawn-dusk direction. For jets smaller than the local Larmor radius in the reconnected magnetic field B_z there is a linear relationship between the width of the jet and the maximum ion outflow velocity inside the jet. At larger widths, the maximum ion outflow velocity then approaches the upstream Alfvén speed. A scaling argument in support of this linear relationship suggests that the slope only depends on the ratio of B_z to the upstream B_x.

The results of this paper could be used to establish the relative positions of satellites with respect to a dipolarization jet as well as placing limits on the cross-tail width of the jet. If the ion flow in the x direction is faster than the local $\mathbf{E} \times \mathbf{B}$ drift, especially in the presence of a reversal in the usual Hall field, the satellite must be on the duskside of the jet and the width must be larger than the scale length $L_y/d_i = \sqrt{n_0/n_b}(B_x/B_z)$. Alternatively, if an ion flow in the x direction is observed without a finite B_z, that would indicate a position duskward of a dipolarization jet. A measured jet outflow velocity well below the upstream Alfvén speed and with $B_z \neq 0$ would suggest that the satellite is on the dawnward side of the jet or that the jet has a very small cross-tail width compared with the effective scale length $L_y/d_i = \sqrt{n_0/n_b}(B_x/B_z)$.

References

Angelopoulos, V., McFadden, J., Larson, D., Carlson, C. W., Mende, S., Frey, H., et al. (2008). Tail reconnection triggering substorm onset. *Science*, *321*, 931–935.

Arzner, K., & Scholer, M. (2001). Kinetic structure of the post plasmoid plasma sheet during magnetotail reconnection. *Journal of Geophysical Research*, *116*, 3827–3844.

Büchner, J., & Zelenyi, L. M. (1989). Regular and chaotic charged particle motion in magnetotaillike field reversals: 1. Basic theory of trapped motion. *Journal of Geophysical Research*, *94*, 11,821–11,842.

Drake, J. F., Swisdak, M., Cassak, P. A., & Phan, T. D. (2014). On the 3-D structure and dissipation of reconnection-driven flow-bursts. *Geophysical Research Letters*, *41*, 3710–3716. https://doi.org/10.1002/2014GL060249

Eastwood, J. P., Phan, T. D., Drake, J. F., Shay, M. A., Borg, A. L., Lavraud, B., & Taylor, M. G. G. T. (2013). Energy partition in magnetic reconnection in Earth's magnetotail. *Physical Review Letters*, *110*, 225001.

Haggerty, C. C., Shay, M. A., Chasapis, A., Phan, T. D., Drake, J. F., Malakit, K., et al. (2018). The reduction of magnetic reconnection outflow jets to sub–Alfvénic speeds arXiv preprint arXiv:1804.09805.

Hietala, H., Drake, J. F., Phan, T. D., Eastwood, J. P., & McFadden, J. P. (2015). Ion temperature anisotropy across a magnetotail reconnection jet. *Geophysical Research Letters*, *42*, 7239–7247. https://doi.org/10.1002/2015GL065168

Le, A., Egedal, J., Daughton, W., Drake, J. F., Fox, W., & Katz, N. (2010). Magnitude of the Hall fields during magnetic reconnection. *Geophysical Research Letters*, *37*, L03106. https://doi.org/10.1029/2009GL041941

Le, A., Egedal, J., Ng, J., Karimabadi, H., Scudder, J., Roytershteyn, V., et al. (2014). Current sheets and pressure anisotropy in the reconnection exhaust. *Physics of Plasmas*, *21*, 012103.

Liu, Y. H., Drake, J. F., & Swisdak, M. (2012). The structure of the magnetic reconnection exhaust boundary. *Physics of Plasmas*, *19*(2), 022110.

Mandt, M. E., Denton, R. E., & Drake, J. F. (1994). Transition to whistler mediated magnetic reconnection. *Geophysical Research Letters*, *21*, 73–76.

Øieroset, M., Phan, T. D., Fujimoto, M., Lin, R. P., & Lepping, R. P. (2001). In situ detection of collisionless reconnection in the Earth's magnetotail. *Nature*, *412*, 414–417.

Parker, E. N. (1957). Sweet's mechanism for merging magnetic fields in conducting fluids. *Journal of Geophysical Research*, *62*, 509–520.

Pritchett, P. L. (2015). Structure of exhaust jets produced by magnetic reconnection localized in the out-of-plane direction. *Journal of Geophysical Research: Space Physics*, *120*, 592–608. https://doi.org/10.1002/2014JA020795

Pritchett, P. L., Coroniti, F. V., & Nishimura, Y. (2014). The kinetic ballooning/interchange instability as a source of dipolarization fronts and auroral streamers. *Journal of Geophysical Research: Space Physics*, *119*, 4723–4739. https://doi.org/10.1002/2014JA019890

Scholer, M., & Lottermoser, R. F. (1998). On the kinetic structure of the magnetotail reconnection layer. *Geophysical Research Letters*, *25*, 3281–3284.

Shay, M. A., Drake, J. F., Eastwood, J. P., & Phan, T. D. (2011). Super-Alfvénic propagation of substorm reconnection signatures and Poynting flux. *Physical Review Letters*, *107*, 065001.

Sitnov, M. I., Merkin, V. G., Pritchett, P. L., & Swisdak, M. (2017). Distinctive features of internally driven magnetotail reconnection. *Geophysical Research Letters*, *44*, 3028–3037. https://doi.org/10.1002/2017GL072784

Sitnov, M. I., Merkin, V. G., Swisdak, M., Motoba, T., Buzulukova, N., Moore, T. E., et al. (2014). Magnetic reconnection, buoyancy, and flapping motions in magnetotail explosions. *Journal of Geophysical Research: Space Physics*, *119*, 7151–7168. https://doi.org/10.1002/2014JA020205

Sitnov, M. I., & Swisdak, M. (2011). Onset of collisionless magnetic reconnection in two-dimensional current sheets and formation of dipolarization fronts. *Journal of Geophysical Research*, *116*, A12216. https://doi.org/10.1029/2011JA016920

Sonnerup, B. U. Ö. (1979). Magnetic field reconnection. *Solar System Plasma Physics*, *3*, 45–108.

Wu, P., & Shay, M. A. (2012). Magnetotail dipolarization front and associated ion reflection: Particle-in-cell simulations. *Geophysical Research Letters*, *39*, L08107. https://doi.org/10.1029/2012GL051486

Zeiler, A., Biskamp, D., Drake, J. F., Rogers, B. N., Shay, M. A., & Scholer, M. (2002). Three-dimensional particle simulations of collisionless magnetic reconnection. *Journal of Geophysical Research*, *107*(A9), 1230.